BAMS Article

Bay of Bengal Intraseasonal Oscillations and the 2018 Monsoon Onset

Emily Shroyer, Amit Tandon, Debasis Sengupta, Harindra J. S. Fernando, Andrew J. Lucas, J. Thomas Farrar, Rajib Chattopadhyay, Simon de Szoeke, Maria Flatau, Adam Rydbeck, Hemantha Wijesekera, Michael McPhaden, Hyodae Seo, Aneesh Subramanian, R Venkatesan, Jossia Joseph, S. Ramsundaram, Arnold L. Gordon, Shannon M. Bohman, Jaynise Pérez, Iury T. Simoes-Sousa, Steven R. Jayne, Robert E. Todd, G. S. Bhat, Matthias Lankhorst, Tamara Schlosser, Katherine Adams, S. U. P Jinadasa, Manikandan Mathur, M. Mohapatra, E. Pattabhi Rama Rao, A. K. Sahai, Rashmi Sharma, Craig Lee, Luc Rainville, Deepak Cherian, Kerstin Cullen, Luca R. Centurioni, Verena Hormann, Jennifer MacKinnon, Uwe Send, Arachaporn Anutaliya, Amy Waterhouse, Garrett S. Black, Jeremy A. Dehart, Kaitlyn M. Woods, Edward Creegan, Gad Levy, Lakshmi H. Kantha, and Bulusu Subrahmanyam

ABSTRACT: In the Bay of Bengal, the warm, dry boreal spring concludes with the onset of the summer monsoon and accompanying southwesterly winds, heavy rains, and variable air–sea fluxes. Here, we summarize the 2018 monsoon onset using observations collected through the multinational Monsoon Intraseasonal Oscillations in the Bay of Bengal (MISO-BoB) program between the United States, India, and Sri Lanka. MISO-BoB aims to improve understanding of monsoon intraseasonal variability, and the 2018 field effort captured the coupled air–sea response during a transition from active-to-break conditions in the central BoB. The active phase of the ~20-day research cruise was characterized by warm sea surface temperature (SST > 30°C), cold atmospheric outflows with intermittent heavy rainfall, and increasing winds (from 2 to 15 m s^{-1}). Accumulated rainfall exceeded 200 mm with 90% of precipitation occurring during the first week. The following break period was both dry and clear, with persistent 10–12 m s^{-1} wind and evaporation of 0.2 mm h^{-1}. The evolving environmental state included a deepening ocean mixed layer (from ~20 to 50 m), cooling SST (by ~1°C), and warming/drying of the lower to midtroposphere. Local atmospheric development was consistent with phasing of the large-scale intraseasonal oscillation. The upper ocean stores significant heat in the BoB, enough to maintain SST above 29°C despite cooling by surface fluxes and ocean mixing. Comparison with reanalysis indicates biases in air–sea fluxes, which may be related to overly cool prescribed SST. Resolution of such biases offers a path toward improved forecasting of transition periods in the monsoon.

KEYWORDS: Atmosphere-ocean interaction; Monsoons; In situ atmospheric observations; In situ oceanic observations

https://doi.org/10.1175/BAMS-D-20-0113.1
Corresponding author: Emily Shroyer, emily.shroyer@oregonstate.edu
In final form 29 April 2021

AFFILIATIONS: Shroyer, de Szoeke, Cherian,* and Cullen—College of Earth, Ocean, and Atmospheric Sciences, Oregon State University, Corvallis, Oregon; **Tandon and Simoes-Sousa**—University of Massachusetts Dartmouth, Dartmouth, Massachusetts; **Sengupta and Bhat**—Indian Institute of Science, Bengaluru, India; **Fernando and Pérez**—University of Notre Dame, Notre Dame, Indiana; **Lucas, Lankhorst, Schlosser, Centurioni, Hormann, MacKinnon, Send, Anutaliya,* and Waterhouse**—Scripps Institution of Oceanography, University of California, San Diego, La Jolla, California; **Farrar, Seo, Jayne, and Todd**—Woods Hole Oceanographic Institution, Woods Hole, Massachusetts; **Chattopadhyay and Sahai**—Indian Institute of Tropical Meteorology, Pune, India; **Flatau**—U.S. Naval Research Laboratory, Monterey, California; **Rydbeck and Wijesekera**—U.S. Naval Research Laboratory, Stennis Space Center, Mississippi; **McPhaden**—NOAA/Pacific Marine Environmental Laboratory, Seattle, Washington; **Subramanian and Kantha**—University of Colorado Boulder, Boulder, Colorado; **Venkatesan, Joseph, and Ramsundaram**—National Institute of Ocean Technology, Chennai, India; **Gordon and Bohman**—Lamont-Doherty Earth Observatory, Columbia University, Palisades, New York; **Adams**—Naval Information Warfare Center Pacific, San Diego, California; **Jinadasa**—Ocean University of Sri Lanka, Colombo, Sri Lanka; **Mathur**—Indian Institute of Technology Madras, Chennai, India; **Mohapatra**—India Meteorological Department, New Delhi, India; **Pattabhi Rama Rao**—Indian National Centre for Ocean Information Services, Hyderabad, India; **Sharma**—Space Applications Centre, Indian Space Research Organisation, Ahmedabad, India; **Lee and Rainville**—Applied Physics Laboratory, University of Washington, Seattle, Washington; **Black, Dehart, and Woods**—53rd Weather Reconnaissance Squadron, U.S. Air Force, Biloxi, Mississippi; **Creegan**—DEVCOM Army Research Laboratory, Adelphi, Maryland; **Levy**—NorthWest Research Associates, Redmond, Washington; **Subrahmanyam**—University of South Carolina, Columbia, South Carolina

*** Current affiliations: Cherian**—National Center for Atmospheric Research, Boulder, Colorado; **Anutaliya**—Institute of Marine Science, Burapha University, Chonburi, Thailand

More than one-third of the world's population lives within the region influenced by the Asian monsoon, where the monsoon is a cornerstone of cultural identity, societal health, and economic security. The boreal spring season is a period of relative calm between the northeasterly winds of the winter (northeast) monsoon and the southwesterly winds of the summer (southwest) monsoon. In late April to early May, the surface temperatures reach a yearly maximum, with sea surface temperature (SST) exceeding 30°C over much of the northern Indian Ocean and daily maximum air temperatures exceeding 40°C over most of India. With the onset of the summer monsoon, southwesterly winds bring moisture-laden air and heavy rains to southern and southeastern Asia, providing a respite from the dry, hot boreal spring. Forecasting of variability in monsoon rainfall is critically important for the region with direct implications for water management policies and implementation of flood and drought mitigation strategies. Precipitation has a direct relation to regional economic prosperity through agricultural production. The gross domestic product of India covaries with rainfall anomalies over ~5% on a year-to-year basis (Gadgil and Rupa Kumar 2006). Production depends not only on the total accumulated rainfall but also on the timing of the abrupt rains accompanying the monsoon onset. The region's reliance on and connection with the monsoon has long been appreciated (Iyengar 2009): "To deluge the earth with generous showers, and the lisping patter of rain, rings sweet to the ears of men" (translation of Kalidasa's *Ritusamhara* from 1792, Pandit 1944; Murty 2014).

At a highly idealized level, the monsoon results from seasonal variation in solar forcing along with the contrasting thermal response of land and ocean. This commonly relied on framework ignores the critical role of moisture (e.g., Chou and Neelin 2003) and overlooks the development of monsoons in aquaplanet simulations (Bordoni and Schneider 2008). Understanding the observed mean monsoon circulation and its variation on intraseasonal to

interannual time scales requires careful consideration of the atmospheric circulation, from regional synoptic weather systems to the equatorial wave band to extratropical connections, and the processes that control exchange of heat, moisture, and momentum at the air–sea and air–land interfaces. The Asian monsoon is thus a result of complex coupled interaction between the atmosphere, ocean, and land, and this complexity presents a direct challenge for forecasting. Although many improvements have been realized over the more than century-long forecasting effort starting with early empirical studies by the India Meteorological Department (IMD; Archibald 1896; Sikka 2011) through to modern dynamical–statistical approaches (e.g., Saha et al. 2019), improving forecast skill of monsoon precipitation remains a fundamental challenge (Gadgil et al. 2005; Mandke et al. 2020).

Forecast fidelity of intraseasonal "active" (wet) and "break" (dry) periods is particularly poor (Neena et al. 2017; Lee et al. 2015). These periods of active and suppressed convection are often associated with large-scale propagating intraseasonal oscillations (ISOs), including the 30–60-day northeastward-propagating boreal summer intraseasonal oscillation (e.g., Jiang et al. 2004) and a 10–20-day westward-propagating mode (e.g., Krishnamurti and Ardanuy 1980). Recent model studies have indicated representation of ISOs is improved when the atmosphere is coupled to the ocean, suggesting a role for air–sea interaction in 10–60-day modulation of the monsoon (DeMott et al. 2014; Fu et al. 2007). Air–sea coupling can influence the intraseasonal signal either directly (e.g., through the phasing of air–sea fluxes, precipitation, and SST) or indirectly through control on the overall atmospheric state, which in turn influences the intraseasonal signal. The relative importance of a direct versus indirect feedback remains an open question (Klingaman and Woolnough 2014) that should be systematically explored (e.g., Klingaman and Demott 2020, show a strong link between ISO representation and ENSO phase in one model). Disentangling this physical dependence is not straightforward, and matters are made more complicated by sensitivity to the coupling approach including resolution and frequency (Klingaman et al. 2011). This sensitivity emphasizes the multiscale nature of intraseasonal variability and highlights the need for high-resolution observations of the ocean and atmosphere in different ISO phases.

The U.S. Office of Naval Research's Monsoon Intraseasonal Oscillations in the Bay of Bengal (MISO-BoB) program was motivated by the need for high-quality, high-resolution observations that span from the upper ocean across the air–sea interface and atmospheric boundary layer into the troposphere during active and break periods of the summer monsoon. The aim of MISO-BoB and associated programs, India's Ocean Mixing and Monsoons and the U.S. Naval Research Laboratory's (NRL) Role of the Indian Ocean on Monsoon Intraseasonal Oscillations, is to understand the ocean's influence on the coupled ocean–atmosphere signal at different spatial and temporal scales. Newly acquired data from both the 2018 and 2019 field seasons are being integrated with process-based models and regional simulations to determine pathways for improvements in representation of the coupled air–sea response.

Within the north-central Bay of Bengal, substantial freshwater from precipitation and rivers creates a shallow low-salinity layer and sharp pycnocline, which modifies the upper ocean's response to atmospheric forcing (Jaeger and Mahadevan 2018; Thakur et al. 2019; Chaudhuri et al. 2019) and allows for development of subsurface warm layers and heat storage (e.g., Sengupta et al. 2008; Thadathil et al. 2016; Shroyer et al. 2016; Lucas et al. 2016). Coupled models tend to show biases in ocean mixed layer depth and SST in this region (Goswami et al. 2016, and references therein). MISO-BoB and partner programs are largely focused on understanding the three-dimensional processes that determine the upper-ocean stratification and heat storage, which in turn influence the atmosphere's intraseasonal variability (e.g., Vecchi and Harrison 2002; Fu et al. 2003; DeMott et al. 2013). Physical processes of interest span both the atmosphere and upper ocean. Ongoing studies rely on observations, realistic models and reanalysis, and idealized modeling (coupled and uncoupled) in order to

detangle complex and interacting processes. Some efforts are focused on improvements to models and products, e.g., intercomparison of modeled and measured fluxes, assessment of oceanic vertical mixing parameterizations, and characterization of the high-resolution structure of cool atmospheric outflows. Other ongoing work is aimed at dynamical understanding of physical processes during the onset and summer monsoon, e.g., exchange of water from the coastal regions into the interior, the oceanic diurnal cycle in the presence of lateral fronts, modulation of the atmospheric boundary layer by ocean fronts, and intraseasonal variability of the land–sea breeze signal. Rather than provide a collection of initial results from these underway efforts, here, we focus on a descriptive summary of the conditions during the first multiweek cruise (4–23 June on board the R/V *Thompson*) of the 2018 MISO-BoB program (Fig. 1).

The 2018 MISO-BoB campaign occurred near the end of the northward progression of the monsoon onset in the central BoB. Here, we use the terminology "onset" to encompass the period of enhanced southwesterly winds that are sustained after the abrupt increase in precipitation in Kerala, which has long been used as an objective measure for onset date (e.g., Ananthakrishnan and Soman 1988). As is typically the case (Goswami 2005), the 2018 onset projected onto the northward propagating Monsoon IntraSeasonal Oscillation (MISO[1]). Accordingly, the early part of the cruise was characterized by active conditions with intermittent, heavy rain, while the latter part of the cruise was relatively clear with little precipitation. In response to the onset, the ocean's mixed layer deepened and SST cooled throughout most of the bay by roughly 1.5°C. Despite persistent winds, SST remained in excess of 29°C well into the summer monsoon season, a reflection of the significant amount of heat stored within the upper ocean above the thermocline.

[1] The MISO index is defined by IMD's analysis of variability in precipitation over India; in many cases, it can be interchanged with ISO, which we use to encompass intraseasonal variability more broadly.

2018 MISO-BoB program

A primary observational challenge of MISO-BoB (Fig. 1) was resolving the range of spatial and temporal scales relevant to intraseasonal activity within the Bay. To address this challenge, the program relied on high-resolution, short-duration sampling embedded within a larger-scale observational framework consisting of the sustained measurements of the Research Moored Array for African–Asian–Australian Monsoon Analysis and Prediction (RAMA; McPhaden et al. 2009) and the Ocean Moored Buoy Network for the Northern Indian Ocean (OMNI; Venkatesan et al. 2013), together with program-supported long-term measurements (e.g., additional moorings, gliders, drifters, and floats).

Ship-based measurements (Fig. 1a) spanned the air–sea interface. The Scripps Institution of Oceanography (SIO) FastCTD (conductivity–temperature–depth) system (Pinkel et al. 2015) sampled temperature, salinity, and optical characteristics to ~200-m depth. Near-surface stratification was sampled at the bow via a weighted line with discretely spaced temperature and salinity sensors. Shipboard Doppler profilers measured upper-ocean currents, and the ship's throughflow system sampled temperature, salinity, and fluorescence via an intake near 4-m depth. Meteorological sensors sampled near-surface winds, temperature, humidity, precipitation, and downward radiative components. Sea surface temperature (see sidebar "Sea surface temperature") was sampled using a floating thermistor (nominally 5-cm depth), and skin temperature was measured by a down-looking radiometer. These data allow for calculation of bulk air–sea fluxes (Fairall et al. 1996, 2003), although direct covariance fluxes were also measured. Rawinsondes were launched at a minimum 12-h interval with supplemental time series of low-level wind profiles (lidar) and cloud height (ceilometer) at higher temporal resolution. Concurrently, air–sea fluxes and upper-ocean evolution were measured from a drifting buoy, which combines a Woods Hole Oceanographic Institution air–sea flux buoy and

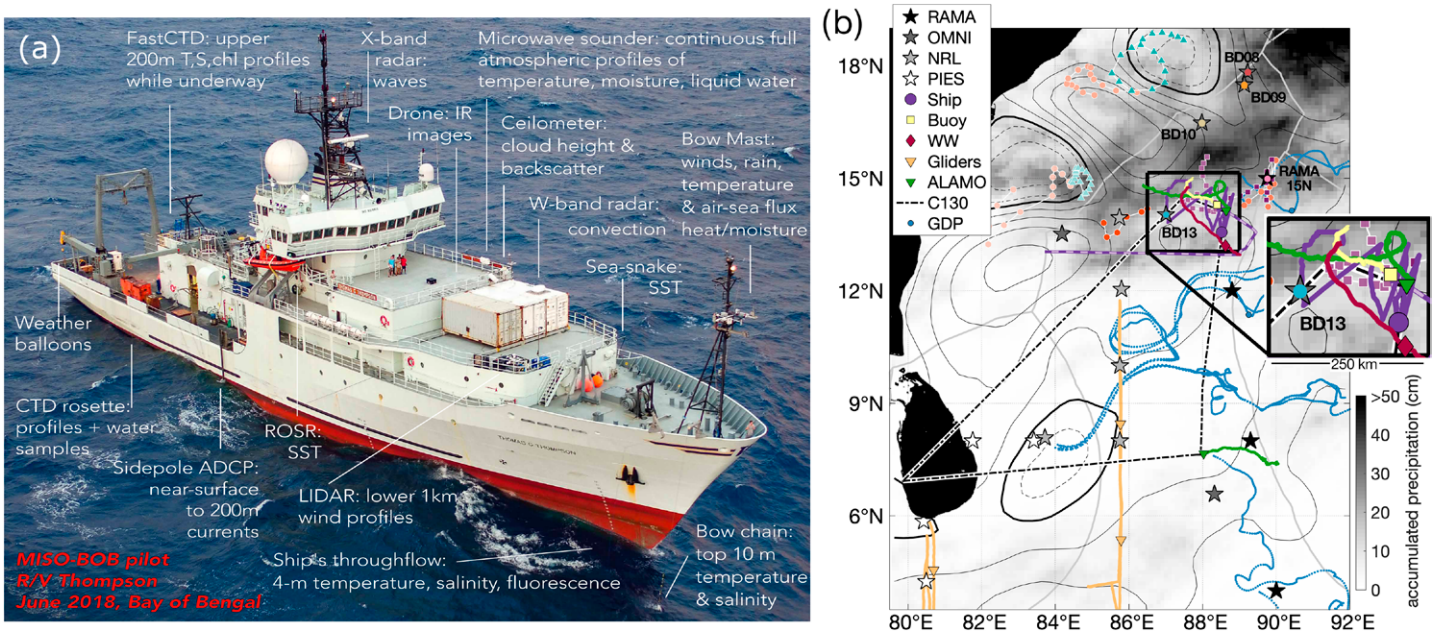

Fig. 1. (a) Drone image of the R/V *Thompson* with sampling tools. (b) Regional map showing accumulated IMERG (Integrated MultisatellitE Retrievals for Global Precipitation Measurement) precipitation over 5–13 Jun 2018 (shading) and Aviso sea surface height anomaly on 10 Jun 2018 (black contours). Nearby the ship (inset), two short-term drifting platforms (air–sea flux buoy in yellow and Wirewalker array in red) formed additional reference points for the ship (purple). Tracks of other mobile assets are limited to sampling during the 2018 southwest monsoon, and markers indicate locations on 18 Jun 2018, after which short-term drifting assets were recovered for the return trip (dashed purple). Argo floats (white-outlined markers) are indicated using the legend shown in sidebar "Transition of the ocean mixed layer into the summer monsoon," and labeled moorings refer to data shown in Fig. 7.

SIO Wirewalker wave-powered profiler within ~50 km of the ship (Fig. 1b).

The above measurements represent a small component of the overall program, which included a second cruise out of Sri Lanka for basinwide NRL mooring deployments, augmentation of land-based radiosonde systems, a joint U.S.–Sri Lankan aircraft effort, and sampling by autonomous platforms (Fig. 1b). A U.S. Air Force WC-130J airplane from the 53rd Weather Reconnaissance Squadron performed a dropsonde survey along the equator, and deployed profiling floats and surface drifters. Several systems were targeted toward a multiyear presence (spanning 2018–19 and in some cases extending earlier). For example, enhancements to the Global Drifter Program

Sea surface temperature

The term "sea surface temperature" can encompass multiple meanings since measurements from different near-surface depths can vary due to the temperature structure over the upper few meters. Following Donlon et al. (2002), the hypothetical interface SST, which is not measurable with available technology, is the temperature in an infinitesimally thin layer at the air–sea interface. The skin SST, measured at depths $O(10–100)$ μm using a radiometer, is typically specified through a measurement wavelength. The skin SST is so named because surface cooling from longwave, sensible, and latent heat loss can cause a "cool skin" over the upper few centimeters, but it can also differ from other definitions of surface temperature because of shallow stratification near the surface, such as when a diurnal warm layer forms under weak winds (e.g., Prytherch et al. 2013; Hughes et al. 2020). The subskin temperature (~1-mm depth) is the temperature at the base of the conductive laminar skin layer. Beneath the subskin, where turbulent processes dominate heat transfer, near-surface temperature measurements are referred to as "bulk" SST, subsurface SST, or surface temperature at depth (Group for High-Resolution Sea Surface Temperature, GHRSST). It is this metric of SST that we refer to in the primary text. Although typically noted in association with a depth, we use the term generically to represent the breadth of platform data presented. In all cases, "SST" is measured as close to the surface as a platform allows spanning from above 1–10-m depth. For the wind speed range characterizing the cruise period, the observed difference between the skin (ship-based radiometer) and <10-m bulk (profiler and bow chain) was typically smaller than 0.2°C.

included barometer-equipped and directional wave spectra drifters in addition to standard surface velocity drifters. Autonomous underwater gliders that were deployed in late May 2018 provided information on the upper-ocean conditions south of the ship in a region where the reversing monsoon currents exchange water between the BoB and the neighboring Arabian Sea (Todd 2020). Drifters coupled with long-term Pressure-Sensing Inverted Echo Sounders (PIES) and glider-transects provide an effective framework for assessing long-term variability in exchange around Sri Lanka (see sidebar "Boundary currents near Sri Lanka").

Linking the Bay's atmospheric state to large-scale conditions

Prior to the 2018 summer monsoon, the winter season was characterized by strong subseasonal activity, including an active ISO and convectively coupled Kelvin waves, with several strong events circumnavigating the globe in upper-level wind anomalies. This state was somewhat unexpected given La Niña conditions, which are usually associated with a weakening ISO in the west and central Pacific Ocean (e.g., Woolnough et al. 2000). The 2018 monsoon onset was initiated by the intraseasonal mode that started to develop in early May

Boundary currents near Sri Lanka

The seasonal boundary currents around Sri Lanka serve as conduits for freshwater out and salty water into the BoB (Jensen et al. 2016; Wijesekera et al. 2015; Anutaliya et al. 2017). Through its contribution to the freshwater budget, this exchange influences the upper-ocean stratification in the interior. A U.S.–Sri Lankan effort to observe this region utilized long-term arrays of moorings, PIES, underwater gliders, and surface drifters (Lee et al. 2016). The multiyear monitoring effort focused on two exchange gates: an east–west section along 8°N and north–south section along 80.5°E (Fig. 1 and Fig. SB1). Integrated volume transport (upper 200 m from PIES and altimetry) and surface currents (blended product from surface drifters, altimetry, and winds; Hormann et al. 2019) highlight seasonal and interannual variability within the boundary current system.

During the summer monsoon, there is southward flow across the eastern section (8°N), fed primarily from the Sri Lanka Dome offshore (Schott et al. 2009; Cullen and Shroyer 2019), as opposed to a continuation of the low-salinity East India Coastal Current (EICC) farther north. The southern section (80.5°E) usually shows eastward flow as part of the Southwest Monsoon Current (SMC; Schott et al. 2009). In 2018, the strongest flow transported 8.4 Sv (1 Sv $\equiv 10^6$ m^3 s^{-1}) southward across 8°N in late June. Eastward transport reached 10 Sv across 80.5°E in early July. The duration of the SMC in 2018 was observed to be shorter than usual, returning to near-zero flow by early September rather than mid-October. Otherwise, the 2018 record is typical in that the timing of the onset and strength of the observed boundary currents fall near the multiyear mean (Fig. SB1).

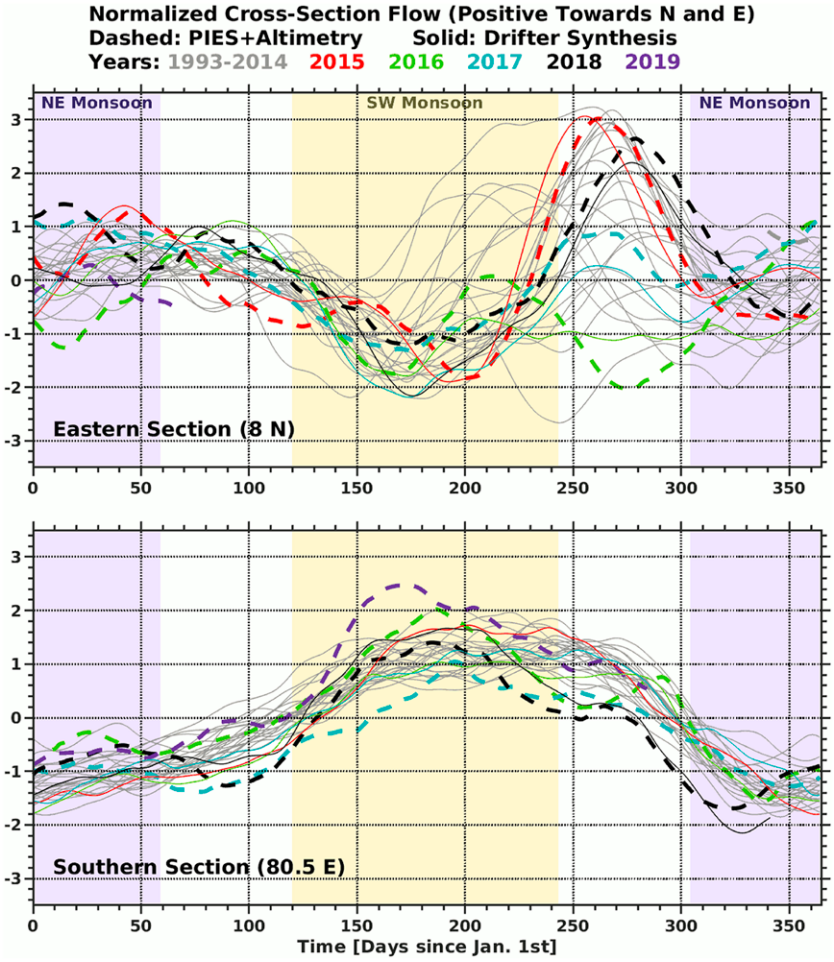

Fig. SB1. Sri Lankan boundary current observations at (top) 8°N and (bottom) 80.5°E. Colors denote different years with 2018 in black. Thick dashed lines are derived from PIES and altimetry; thin solid lines denote the drifter synthesis. All time series were processed with a 45-day moving-average filter, removal of mean values, and normalization by respective standard deviations.

in the central equatorial Indian Ocean (Figs. 2a,b). By the end of May, the northward shift of convection into the BoB (Fig. 2c) led to the subsequent rapid advance of precipitation over much of the Indian Subcontinent. With the onset over Kerala declared on 29 May, the 2018 onset was close to the average date of 1 June (Puranik et al. 2013). The monsoon progressed steadily through West Bengal, Odisha, and Chhattisgarh from 9 to 12 June. After this period, intraseasonal activity subsided, and the monsoon progress weakened considerably from mid- to late June (Fig. 2a). In July and August, BoB intraseasonal activity was reduced (Fig. 2b), as anomalously enhanced convection shifted toward the Pacific Ocean.

India received 91% of its June–September climatological rainfall in 2018 (IMD's 2018 End of Season Report), characterizing the year as normal (within one standard deviation). Once

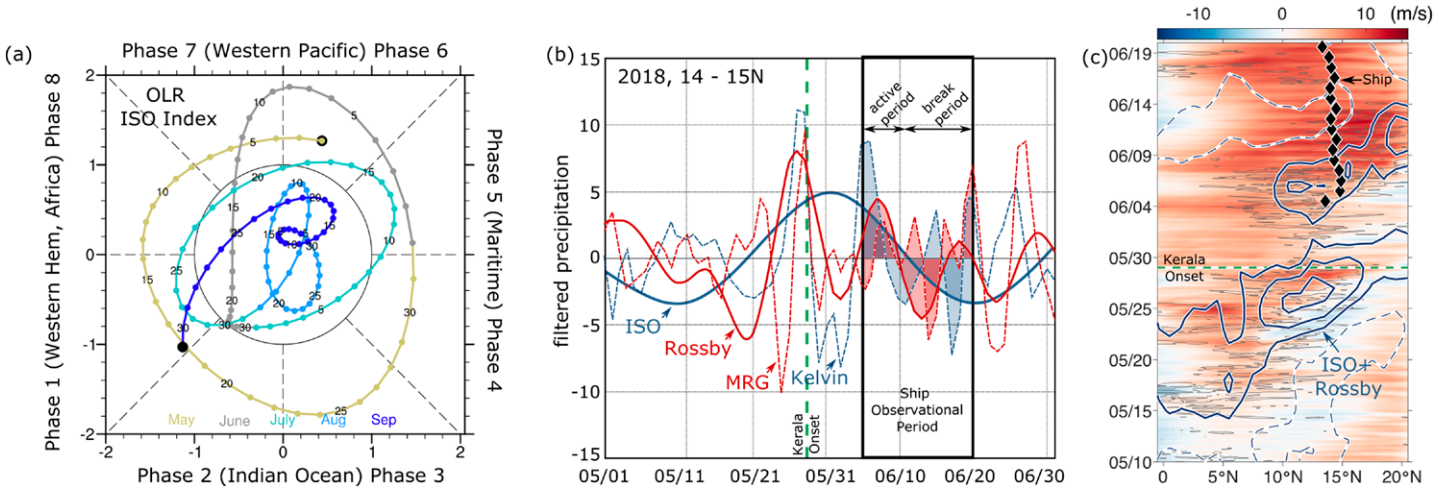

Fig. 2. (a) ISO phase and amplitude for 2018 (Kiladis et al. 2014). (b) Decomposition of precipitation anomaly (mm day^{-1}) during May and June of 2018 for the ISO (blue solid), Kelvin (blue dashed), Rossby (red solid), and mixed Rossby–gravity waves (red dashed). Anomalies are identified using wavenumber and frequency over 14°–15°N, 85°–90°E, the approximate position of the ship. Shading highlights when modes "constructively" and "destructively" interfere during the cruise period. (c) ERA5 eastward 10-m winds (shading) averaged over 85°–90°E. Gray contours highlight regions where the total hourly ERA5 precipitation exceeds 15 mm; white–blue contours are the filtered Rossby and ISO modes from (b), with positive anomalies as solid lines.

the monsoon developed (30 May forecast, Fig. 3), IMD's operational forecast system skillfully predicted its northward propagation, as measured by the MISO index (Suhas et al. 2013). Forecasting skill was limited during the initial intensification of the ISO (15 May forecast, Fig. 3) as well as for higher-frequency variability (the 6 June forecast, Fig. 3 and Fig. 2b). Accurate projection of regional precipitation requires high forecasting skill of both MISO initiation and propagation, as well as representation of higher-frequency systems within.

A local perspective of the onset and transition from active and break conditions

Atmospheric evolution. Within the MISO-BoB observational region (Fig. 1b), the intraseasonal signal was accompanied by convectively coupled equatorial modes, which constructively interfered to produce elevated precipitation during the active phase early in the cruise (Figs. 2b,c). Regionally, the active phase (nominally prior to 13 June) was associated with relatively warm (Figs. 4a and 5a), moist (Fig. 5b) air in the midtroposphere. Low-level convergence in the northern Bay, which can be seen from 1,000-hPa wind fields (Figs. 4c), is consistent with ship-based measurements of high clouds (Fig. 5a) and enhanced precipitation (Figs. 5b and 5f). Local moistening of the lower troposphere (1,000–850 hPa, Fig. 5b) started from 6 June with a peak on 10 June in the midtroposphere (~600 hPa, Fig. 5), suggestive of

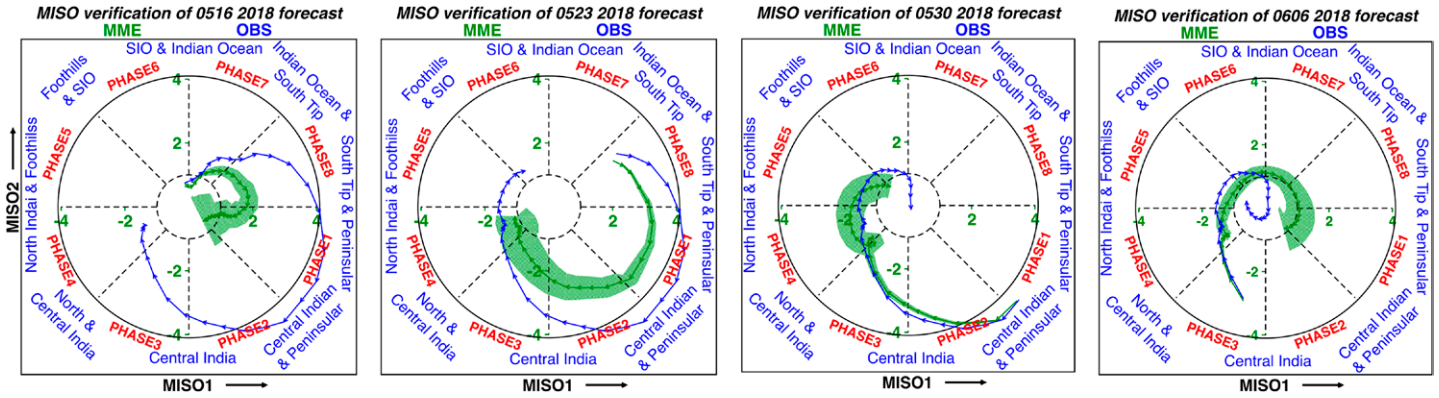

Fig. 3. Operational MISO tracking (blue) and forecast (green) based on Indian Institute of Tropical Meteorology's multimodel ensemble (MME) with forecast initialization date increasing to the right. Solid green tracks the evolution of the ensemble mean (line) and spread (shading). The forecast is based on a multimodel super-ensemble generated from the NCEP (U.S.) CFSv2 coupled model (Saha et al. 2014; Sahai et al. 2019). Each submodel is run with four initial conditions obtained by perturbing the tendency terms in the initial conditions (Abhilash et al. 2013).

upward moisture transport by convection. Following the moistening and warming of the local atmosphere and deep convection, much of the bay experienced enhanced precipitation and reduced convective available potential energy (CAPE).

In contrast, the break phase was associated with cool, dry air aloft (Figs. 4a and 5a,b). Over this time, precipitation was isolated near the BoB's eastern boundary (Figs. 4d), where orographic lifting of the moisture-laden southwest monsoon wind controls precipitation (Xie et al. 2006). A low-level divergence (Fig. 4d) coincided with a reduction of moisture during break conditions in the northern bay (Fig. 5b), consistent with previous work that shows a relationship between divergence and precipitation (Graham and Barnett 1987; Zhang et al. 2018). Clouds during the break period tended to be low and optically thin relative to earlier in the cruise (Fig. 5a). A significant build-up of CAPE from the active to break phase occurs over the northern bay (Figs. 4a,b), consistent with previous observations (Bhat et al. 2001).

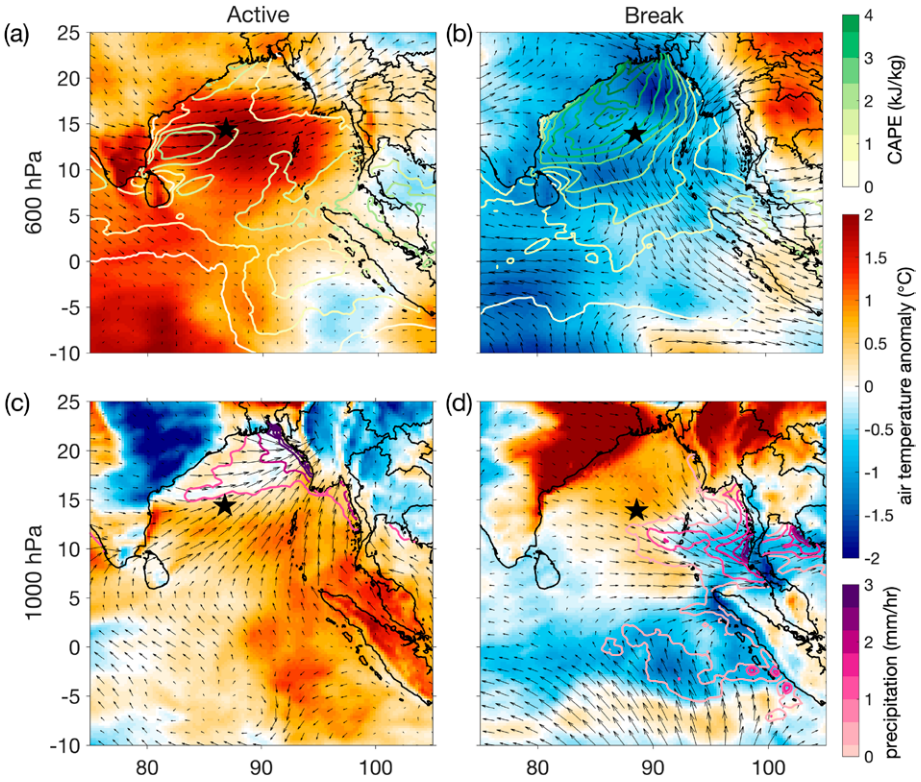

Fig. 4. ERA5-based atmospheric conditions during active (9–12 Jun) and break (16–19 Jun) periods in the north-central bay, showing anomalous air temperature (shading) and winds (vectors) in the (a),(b) midtroposphere and (c),(d) near-surface. Contours show convective available potential energy (CAPE) in (a) and (b) and precipitation in (c) and (d).

Air–sea exchange. Over the cruise duration, the ocean cooled by roughly 50 W m^{-2}, with the net

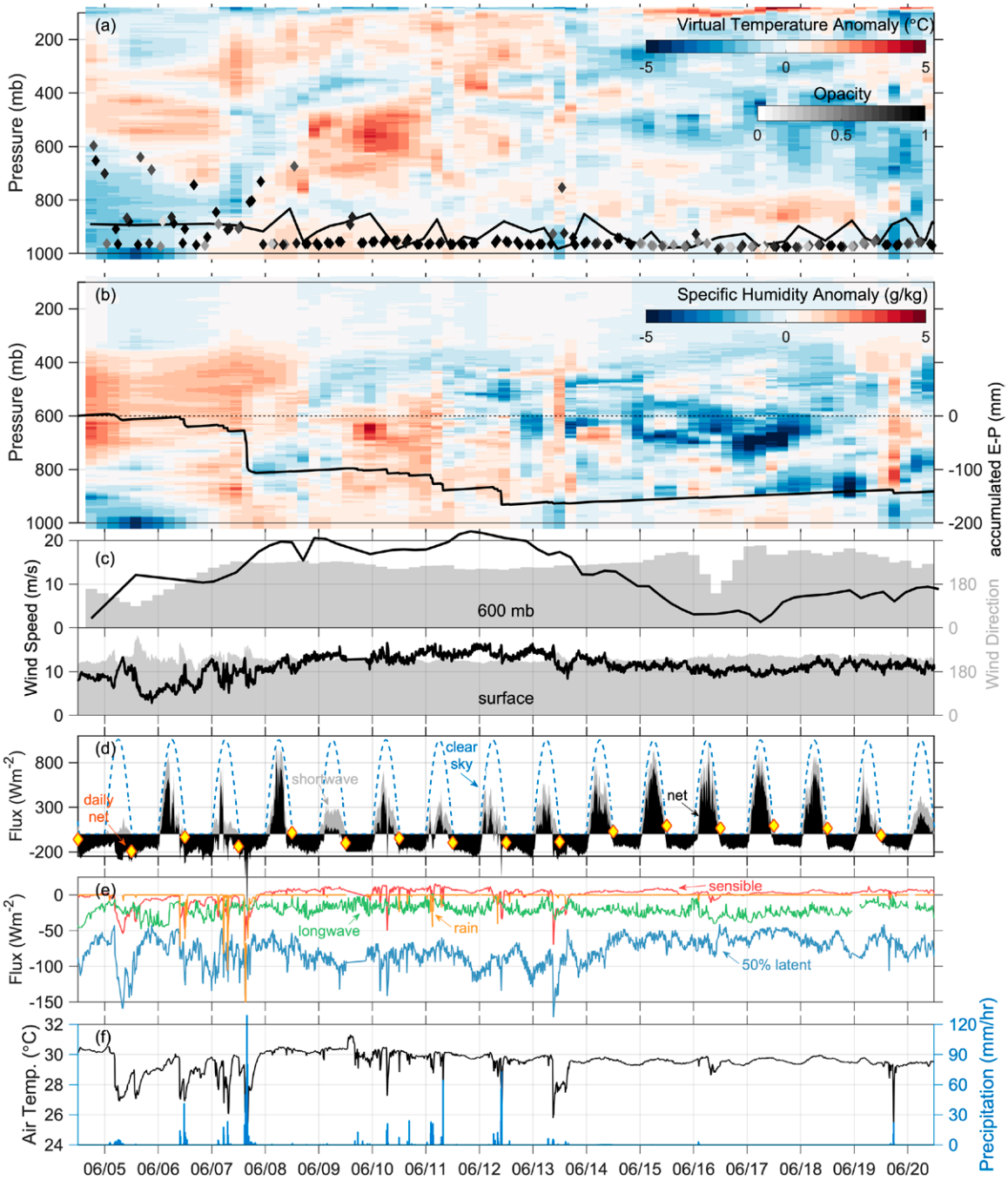

Fig. 5. Ship meteorological fields include (a) virtual temperature anomaly with mean cloud height (diamonds shaded by opacity) and the planetary boundary layer height (black) (Holzworth 1967; Stull 1991); (b) specific humidity anomaly overlaid with cumulative evaporation less precipitation; (c) wind speed (black, LHS) and direction (gray, RHS) (bottom) near the surface and (top) at 600 hPa; (d) net surface flux (10 min in black, daily as diamonds), solar radiation (gray), and clear-sky radiation (blue); (e) other surface flux terms: latent (blue scaled by 50%), sensible (red), longwave (green), rain (yellow), and (f) near-surface air temperature (black, LHS) and precipitation (blue, RHS). Surface fields represent 10-min averages, and atmospheric anomalies from the time mean are interpolated from 2–4-times-daily radiosondes.

heat loss greatest during the active period when insolation was typically much less than the clear-sky value (Fig. 5d). The net surface heat flux cooled the ocean at an average daily rate of −83 W m^{-2} over 4–13 June, and warmed the ocean at an average daily rate of 69 W m^{-2} over 14–18 June. The SST reduced roughly 1.5°C over the cruise (Fig. 6b). Consistent with the large-scale view (Fig. 4c,d), the observed 10-min wind speed (Fig. 5c)

increased to 15 m s^{-1} (stress > 0.3 N m^{-2}) for several days before relaxing to a steady 10 m s^{-1} (0.15 N m^{-2}).

The surface meteorological record is punctuated by cold atmospheric outflows, often accompanied by significant precipitation (Fig. 5f). During these events, the typically southwesterly winds often rotated (Fig. 5c) and the specific humidity dropped (dry outflows, not shown). These events were common during the active period. The 10-min precipitation rate reached 120 mm h^{-1} during one event. The cruise-mean precipitation rate (0.55 mm h^{-1}) was more than twice the evaporation rate (0.20 mm h^{-1}), resulting in a local loss of moisture from the atmosphere (140 mm over the duration of the cruise, Fig. 5b).

Oceanic evolution. Initially, salinity stratification created a shallow ocean mixed layer (OML ~20 m, Fig. 6d). Below, a 50-m-deep barrier layer (separation between the OML and deeper thermocline) contained water 0.5°–1°C warmer than the surface (Fig. 6c). Pronounced layering in temperature and salinity was seen throughout the barrier layer at vertical scales of 10 m and smaller (Figs. 6c,d), accompanied by patches of low Richardson number (ratio of the square of stratification to the square of vertical shear, Fig. 6e) indicating the potential for shear-driven turbulent mixing. By the conclusion of the cruise, the barrier layer had been destroyed, and the temperature-stratified OML base deepened to roughly 50 m (Fig. 6c). This transition occurred over a ~3–4-day period as the winds increased (Fig. 5c).

As the monsoon winds gained strength, the barrier layer insulated the surface from cooler thermocline waters and provided a source of heat that dampened the response of SST to surface cooling. The buoy and ship SST remained steady at close to 30.5°C for several days (Fig. 6b) despite net surface heat loss of –105 W m^{-2} (4–7 June, Fig. 6a) and a deepening OML (Fig. 6f). The erosion of the barrier layer (10 June, Figs. 6c,d) allowed entrainment of cool thermocline water into the mixed layer. Subsequently, SST rapidly cooled (10–11 June,

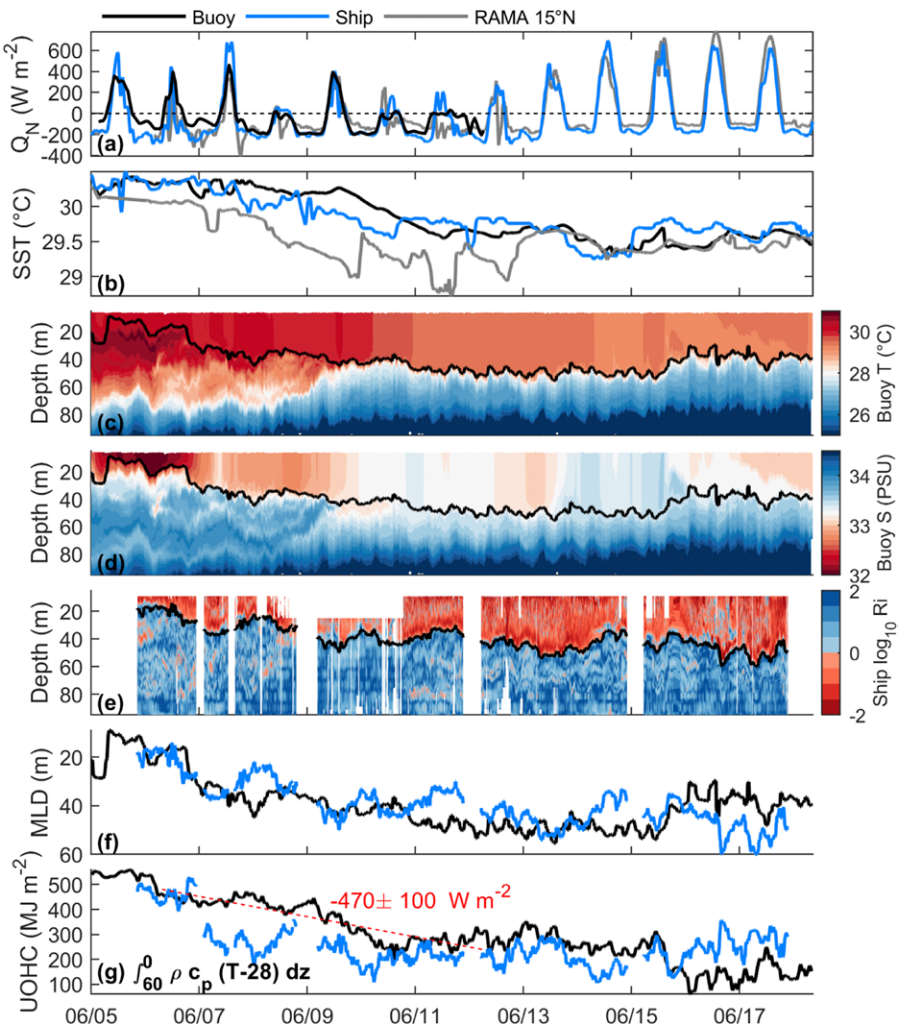

Fig. 6. (a) Net surface heat flux and (b) SST at the buoy (black), ship (blue), and 15°N RAMA mooring (gray). Subsurface (c) temperature and (d) salinity from the buoy, and (e) Richardson number (Ri) at the ship. The (f) MLD and (g) upper-ocean heat content above 28°C, integrated over the upper 60 m from the buoy and ship. A linear fit to heat content from 7 to 12 Jun (red dashed) indicates a daily heat loss of 470 W m^{-2}, where the average heat loss was 100 W m^{-2} larger (smaller) if the 6-day segment was shifted 1 day earlier (later).

Figs. 6a,b). With the transition to daily net heating (13 June) and a deeper OML, SST remained steady close to 29.5°C later in the cruise (Figs. 6a,b). While some variation in OML depth and SST is apparent between the buoy and ship, overall their evolution was remarkably similar (Figs. 6b,f) across the ~75-km scale of the array. Initially, the RAMA mooring at 15°N, about 150 km from the array in a region of greater accumulated precipitation (Fig. 1b), measured SST roughly 1°C cooler (Fig. 6b), but its SST also eventually equilibrated near 29.5°C matching that near the ship.

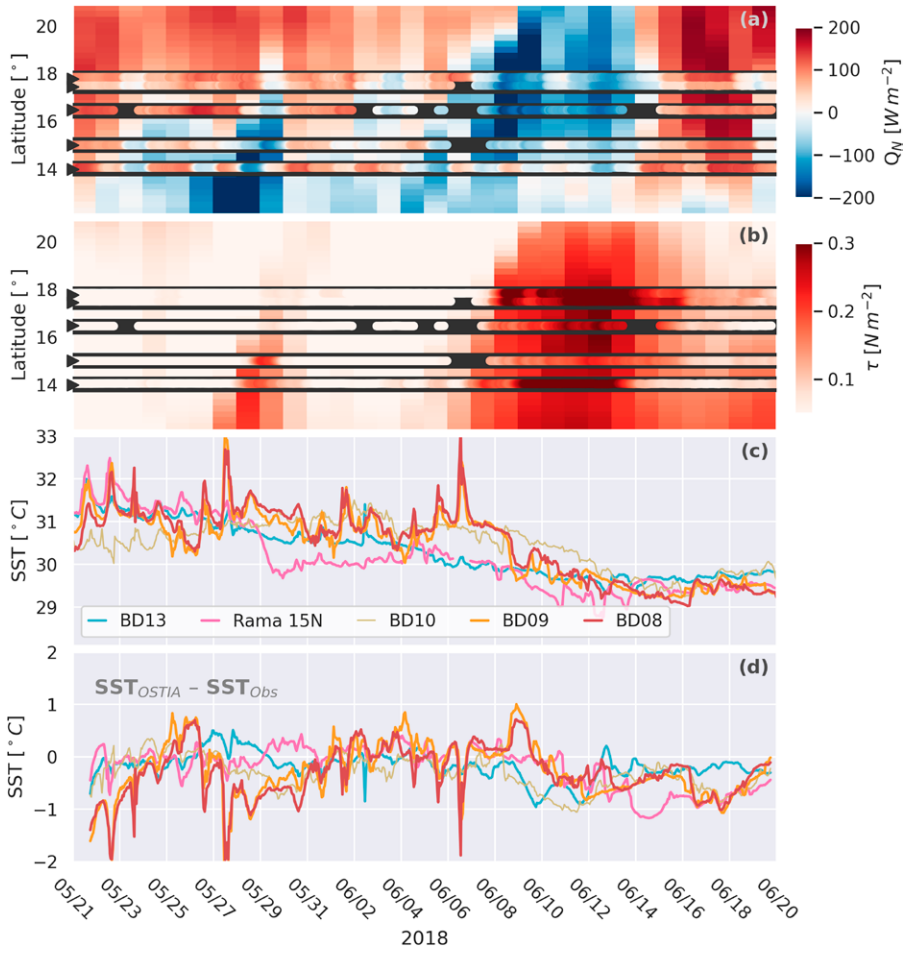

Fig. 7. (a) Net surface heat flux, (b) wind stress, (c) SST, and (d) difference between OSTIA and moored SST. In (a) and (b), daily ERA5 fields (mean over 87–91°E) are overlaid with moored data (spanned by black horizontal lines and marked by arrows to left). Missing mooring data appears as black sections. Time series are ordered by latitude with the southernmost mooring to the left in the legend (as indicated in Fig. 1b). OSTIA's foundation SST should be comparable to the predawn bulk SST of moored time series.

Observations during the MISO-BoB intensive operational period are contextualized by the basin-wide moored array (Fig. 7). The northward progression of the onset was discernible in both decreasing net surface heat flux (Fig. 7a) and increasing southwesterly winds (Fig. 7b). SST cooled by almost 2°C from late May steadying near 29.5°C in late June across the array (Fig. 7c). Diurnal SST anomalies, which reached 1°–2°C in late May, were negligible during the strong wind conditions characterizing the cruise period (Fig. 7c). In the northern Bay, differences in OML depth attributable to mesoscale eddies manifested as comparatively subtle variations in SST (within 0.5°C) relative to the overall cooling during the onset (see sidebar "Transition of the ocean mixed layer into the summer monsoon").

Comparing observations and reanalysis

ERA5 (Hersbach et al. 2020) showed a persistent bias compared to the in situ MISO-BoB observations: reanalysis air temperature was too cool (~2°C), wind stress was too weak (max near 0.2 N m^{-2} as opposed to >0.3 N m^{-2}), and heat fluxes were too high. The cruise-average shortwave was too high by 30 W m^{-2} in ERA5, compensated by reanalysis longwave and sensible fluxes that were too strong by 15 and 7 W m^{-2}, respectively. Measured latent cooling of –155 W m^{-2} was similar to the reanalysis estimate of –158 W m^{-2}. These tendencies are generally consistent with adjustments to the atmospheric boundary layer expected over a prescribed SST that is too cool, i.e., stable boundary with reduced cloud cover and reduced momentum flux from strong winds aloft.

ERA5 relies on the Operational Sea Surface Temperature and Sea Ice Analysis (OSTIA[2]) foundation SST (Donlon et al. 2012). The MISO-BoB observations show that OSTIA SST was too cool 97% of the time, being low by more than 0.75°C (1°C) for 32% (13%) of the ship's record length. Over the observational period, OSTIA SST was biased low by 0.65°C in the cruise average.[3] This tendency for cool bias was not isolated to the ship region, but extended across the moored array over mid- to late June (Fig. 7d). Using all available SST estimates (floats, gliders, moorings, ship, and drifters), it appears that the OSTIA cool bias is limited to the central Bay during the ship observational period (Figs. 7 and 8).

Although OSTIA SST approaches magnitudes close to 28°C (Fig. 8b), a commonly applied threshold above which atmospheric convection is insensitive to SST (Gadgil et al. 1984), the observed upper-ocean temperature exceeded 28°C over the upper 40–80 m (Fig. 6c). This layer represents a substantial heat reservoir available for the atmosphere to tap into during the onset of the summer monsoon. For example, the upper 60 m of the ocean lost approximately 300 MJ m^{-2} of heat over the first week of the cruise. This loss of heat is equivalent to a cooling rate of many hundreds of watts per square meter (Fig. 6g), more than twice the magnitude of the peak daily net surface cooling. Consideration of the uniformity of SST cooling over a broad area combined with the subsurface evolution near the ship suggests turbulent mixing transports significant heat downward to the subsurface ocean during the monsoon onset. However, despite this rapid heat loss, the upper-ocean heat content relative to 28°C remains high at the end of the measurement period (~200 MJ m^{-2}) (Fig. 6g). The ocean would need to continue to lose heat at a rate of ~50 W m^{-2} (cruise-average rate) for more than one month to reach the 28°C threshold below which SST becomes an important factor in convection.

[2] OSTIA combines satellite data with in situ observations to determine a daily sea surface temperature estimate on a 1/20° spatial grid.

[3] OSTIA's "foundation" SST represents a bulk mixed-layer temperature without the very near-surface signals associated with the diurnal warm layer and the cool-skin effect. We did not attempt to remove the diurnal warm layer signal in the ship records, because it is too weak (~0.1°C) to account for the difference.

Conclusions

The results presented here are designed to showcase both the resources collected under MISO-BoB and partner programs as well as the qualitative complexity of the observed monsoon development. To our knowledge, this is the first ship-based record capturing the Bay's transition during the onset, and these observations point suggestively toward targets for additional analysis. In this example, the presence of a subsurface temperature maximum provides a significant heat reservoir. This reservoir results in a lagged response of SST to intense

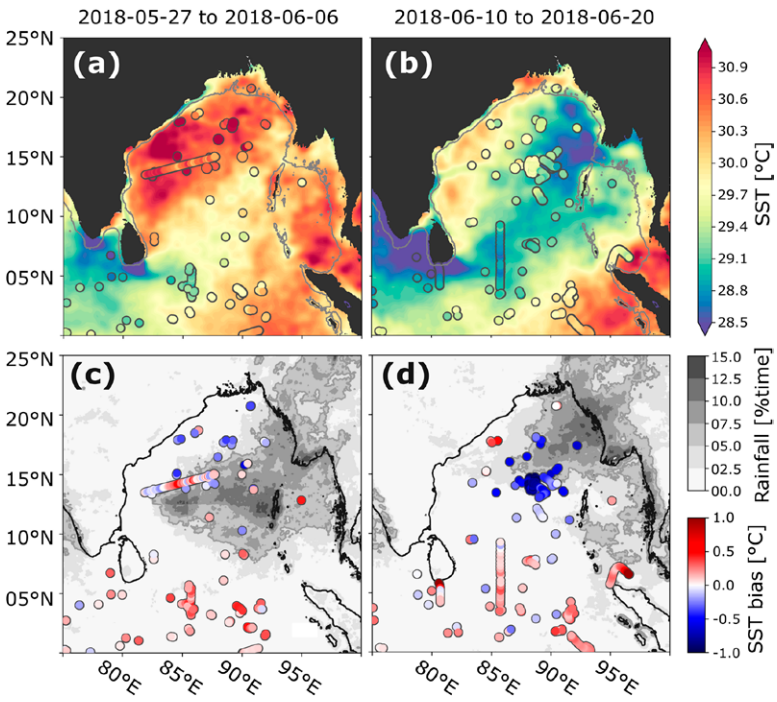

Fig. 8. (a),(b) Comparison between OSTIA foundation (shading) and observed (colored circles) SST. (c),(d) IMERG-derived rainfall (Huffman et al. 2015) in percentage of time (grayscale) and OSTIA SST bias (colored circles). Blue circles indicate OSTIA SST colder than observations. Columns show temporal averages over (left) 27 May–6 Jun and (right) 10–20 Jun. Observational assets have varying temporal resolution from sub-minute (ship) to 10-day increments (Argo). While the observational mean includes diurnal heating, the signal is small during the period of large bias (Figs. 6b and 7c).

Transition of the ocean mixed layer into the summer monsoon

Argo profiles obtained during the spring to summer transition (May–July 2018) in the central and western BoB provide a regional view of the changing OML properties as monsoon winds increase. The measured density profiles (Fig. SB2, top panels) reveal a wide range of values mainly in the 40–120-m depth interval marking the pycnocline. The depth of maximum pycnocline strength occurs near 20–40 m for the shallower pycnocline profiles, and 60–90 m for the deeper pycnocline profiles. As expected the shallower (deeper) pycnocline is related to lower (higher) steric height, marking cyclonic (anticyclonic) eddy features.

The mixed layer depth (MLD) increases from May into July, with the increase occurring during higher winds (Fig. SB2d). However, the MLD increase for a particular float depends on the initial pycnocline structure and barrier layer strength, which inhibits mixing of cool thermocline waters into the OML. Floats associated with higher steric (dynamic) height of the sea surface relative to 180 m develop deeper MLD by July (e.g., Argo ID 233, 234, and 264 in Fig. SB2e). Analogously, floats with lower steric height, e.g., Argo ID 154, 192, and 197, are associated with shallower MLD. Note that Argo floats do not simply capture the 1D stratification, as their parking depth is likely displaced from the overlying water column. For example, Argo ID 230 captured more of a hybrid relation of MLD to steric height, as the float shifted from high to low steric height.

Consistent with the observed broadscale cooling, the sea surface temperature (SST; Fig. SB2f), shows a weak relationship to the steric height and MLD relative to the overall change in SST (roughly 2°C) that occurs with the onset of the monsoon. The MLD increased from May through July 2018 under strong wind forcing, leading to cooling by entrainment that is insufficient to account for the overall reduction in SST from May through July. Additional sea to air heat flux is required, and more ocean heat removal is required for anticyclonic features as compared to cyclonic features. This is perhaps most readily apparent in the roughly 0.5°C spread at the end of the record shown in Fig. SB2 with slightly warmer (cooler) cyclonic (anticyclonic) features. In this way, the atmosphere "sees" (via air–sea heat flux) the ocean eddies.

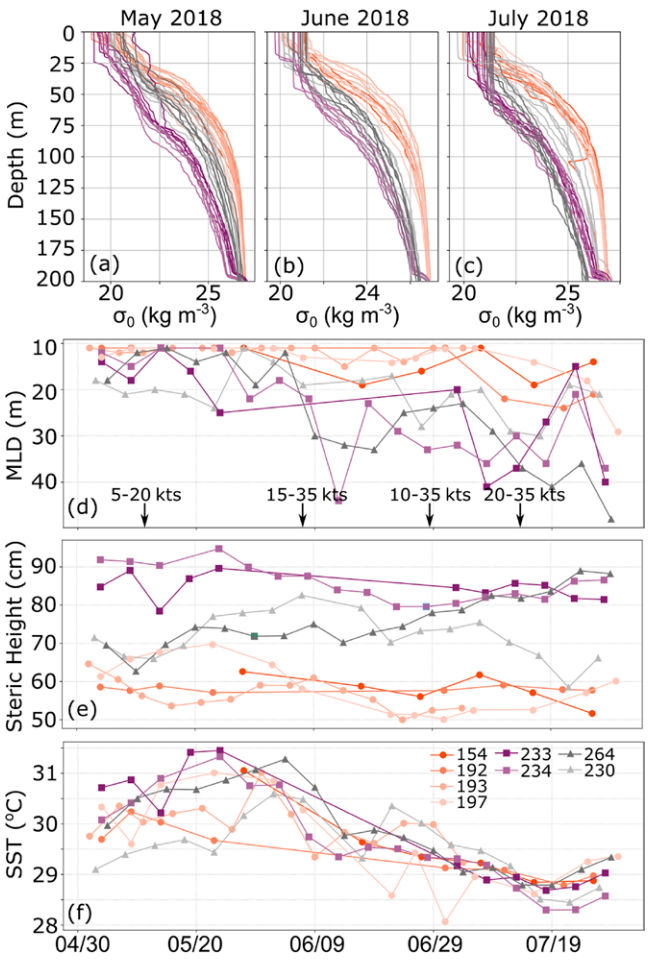

Fig. SB2. (a)–(c) Measured Argo density profiles sorted by month, (d) MLD defined using a 0.03 kg m^{-3} threshold and 10-m intervals (de Boyer Montégut et al. 2004), (e) sea surface relative to 180-m steric (dynamic) height, and (f) 10-m SST from Argo floats. Wind speed (ASCAT 25-km resolution) over the western BoB at specific times is indicated in (d). Floats sampling cyclones (circles) and anticyclones (squares) have relatively low and high dynamic heights, respectively. Two floats (triangles) drifted between cyclones and anticyclones.

surface cooling by several days, and it is substantial enough to keep SST above 29°C during the sampled active and break phases (Figs. 5 and 6). An open dynamical question is the relative role of one-dimensional processes (e.g., penetrating solar radiation, cooling in the presence of salinity stratification, freshwater capping by precipitation) versus three-dimensional processes (e.g., subduction and lateral stirring) in forming and maintaining this structure. These observations also demonstrate that SST has a similar evolution across multiple assets

up to hundreds of kilometers apart (Figs. 7 and 8). That geographic coherence points to the likely uniformity of the subsurface heat reservoir and suggests the relative importance of one-dimensional processes in modifying heat content, *at least at this time of year*. The observed heat loss can only be accounted for through mixing of heat to depth, the consequences of which need to be studied further particularly in the context of heat availability during ISO transitions and later within the fall cyclone season. These observations contrast with the situation later in the monsoon, when lateral gradients in SST are more pronounced and three-dimensional, submesoscale processes play a comparatively larger role in setting upper-ocean stratification (e.g., MacKinnon et al. 2016; Jaeger and Mahadevan 2018; Sree Lekha et al. 2018; Ramachandran et al. 2018). The incorporation of newly available observations and an understanding of the spatial footprint of the Bay's upper-ocean heat content offers the potential to improve our understanding of how the ocean imprints on monsoon variability and vice versa.

Acknowledgments. This work was supported through the U.S. Office of Naval Research's Departmental Research Initiative: Monsoon Intraseasonal Oscillations in the Bay of Bengal, the Indian Ministry of Earth Science's Ocean Mixing and Monsoons Program, and the Sri Lankan National Aquatic Resources Research and Development Agency. We thank the Captain and crew of the R/V *Thompson* for their help in data collection. Surface atmospheric fields included fluxes were quality controlled and processed by the Boundary Layer Observations and Processes Team within the NOAA Physical Sciences Laboratory. Forecast analysis was completed by India Meteorological Department. Drone image was taken by Shreyas Kamat with annotations by Gualtiero Spiro Jaeger. We also recognize the numerous researchers who supported cruise- and land-based measurements. This work represents Lamont-Doherty Earth Observatory contribution number 8503, and PMEL contribution number 5193.

Data availability statement. Community supported data are available from disc.sci.gsfc.nasa.gov (IMERG data, NASA's Global Precipitation Mission), cds.climate.copernicus.eu (ERA5 data, European Centre for Medium-Range Weather Forecasts), urs.earthdata.nasa.gov (OSTIA data, Group for High Resolution Sea Surface Temperature), argo.ucsd.edu and www.ocean-ops.org (International Argo Program), and www.pmel.noaa.gov/tao/gtmba/ (RAMA data, Global Tropical Moored Buoy Array). Project-supported data are embargoed under agreement between the U.S. and India until 2025 as one step in fostering the international collaboration. This time frame is intended to allow for students and postdoctoral researchers supported under the project to have sufficient time to publish observation-based results. After the embargo period, data may be requested from the corresponding author.

References

Abhilash, S., A. K. Sahai, S. Pattnaik, and S. De, 2013: Predictability during active break phases of Indian summer monsoon in an ensemble prediction system using climate forecast system. *J. Atmos. Sol.-Terr. Phys.*, **100–101**, 13–23, https://doi.org/10.1016/j.jastp.2013.03.017.

Ananthakrishnan, R., and M. Soman, 1988: The onset of the southwest monsoon over Kerala: 1901–1980. *J. Climatol.*, **8**, 283–296, https://doi.org/10.1002/joc.3370080305.

Anutaliya, A., and Coauthors, 2017: An undercurrent off the east coast of Sri Lanka. *Ocean Sci.*, **13**, 1035–1044, https://doi.org/10.5194/os-13-1035-2017.

Archibald, D., 1896: The long period weather forecasts of India. *Nature*, **55**, 85–88, https://doi.org/10.1038/055085b0.

Bhat, G. S., and Coauthors, 2001: BOBMEX: The Bay of Bengal Monsoon Experiment. *Bull. Amer. Meteor. Soc.*, **82**, 2217–2244, https://doi.org/10.1175/1520-0477(2001)082<2217:BTBOBM>2.3.CO;2.

Bordoni, S., and T. Schneider, 2008: Monsoons as eddy-mediated regime transitions of the tropical overturning circulation. *Nat. Geosci.*, **1**, 515–519, https://doi.org/10.1038/ngeo248.

Chaudhuri, D., D. Sengupta, E. D'Asaro, R. Venkatesan, and M. Ravichandran, 2019: Response of the salinity-stratified Bay of Bengal to Cyclone Phailin. *J. Phys. Oceanogr.*, **49**, 1121–1140, https://doi.org/10.1175/JPO-D-18-0051.1.

Chou, C., and J. D. Neelin, 2003: Mechanisms limiting the northward extent of the northern summer monsoons over North America, Asia, and Africa. *J. Climate*, **16**, 406–425, https://doi.org/10.1175/1520-0442(2003)016<0406:MLTNEO>2.0.CO;2.

Cullen, K., and E. L. Shroyer, 2019: Seasonality and interannual variability of the Sri Lanka dome. Deep-Sea Res. Part II, 168, 104642, https://doi.org/10.1016/j.dsr2.2019.104642.

de Boyer Montégut, C., G. Madec, A. S. Fischer, A. Lazar, and D. Iudicone, 2004: Mixed layer depth over the global ocean: An examination of profile data and a profile-based climatology. *J. Geophys. Res.*, **109**, C12003, https://doi.org/10.1029/2004JC002378.

DeMott, C. A., C. Stan, and D. A. Randall, 2013: Northward propagation mechanisms of the boreal summer intraseasonal oscillation in the ERA-Interim and SP-CCSM. *J. Climate*, **26**, 1973–1992, https://doi.org/10.1175/JCLI-D-12-00191.1.

——, ——, ——, and M. D. Branson, 2014: Intraseasonal variability in coupled GCMs: The roles of ocean feedbacks and model physics. *J. Climate*, **27**, 4970–4995, https://doi.org/10.1175/JCLI-D-13-00760.1.

Donlon, C. J., P. J. Minnett, C. Gentemann, T. J. Nightingale, I. J. Barton, B. Ward, and M. J. Murray, 2002: Toward improved validation of satellite sea surface skin temperature measurements for climate research. *J. Climate*, **15**, 353–369, https://doi.org/10.1175/1520-0442(2002)015<0353:TIVOSS>2.0.CO;2.

——, M. Martin, J. Stark, J. Roberts-Jones, E. Fiedler, and W. Wimmer, 2012: The Operational Sea Surface Temperature and Sea Ice Analysis (OSTIA) system. *Remote Sens. Environ.*, **116**, 140–158, https://doi.org/10.1016/j.rse.2010.10.017.

Fairall, C. W., E. F. Bradley, D. P. Rogers, J. B. Edson, and G. S. Young, 1996: Bulk parameterization of air-sea fluxes for tropical ocean-global atmosphere coupled-ocean atmosphere response experiment. *J. Geophys. Res.*, **101**, 3747–3764, https://doi.org/10.1029/95JC03205.

——, E. F. Bradley, J. E. Hare, A. A. Grachev, and J. B. Edson, 2003: Bulk parameterization of air–sea fluxes: Updates and verification for the COARE algorithm. *J. Climate*, **16**, 571–591, https://doi.org/10.1175/1520-0442(2003)016<0571:BPOASF>2.0.CO;2.

Fu, X., B. Wang, T. Li, and J. P. McCreary, 2003: Coupling between northward-propagating, intraseasonal oscillations and sea surface temperature in the Indian Ocean. *J. Atmos. Sci.*, **60**, 1733–1753, https://doi.org/10.1175/1520-0469(2003)060<1733:CBNIOA>2.0.CO;2.

——, B. Wang, D. E. Waliser, and L. Tao, 2007: Impact of atmosphere—Ocean coupling on the predictability of monsoon intraseasonal oscillations. *J. Atmos. Sci.*, **64**, 157–174, https://doi.org/10.1175/JAS3830.1.

Gadgil, S., and K. Rupa Kumar, 2006: The Asian monsoon—Agriculture and economy. *The Asian Monsoon*, B. Wang, Ed., Springer, 651–683.

——, P. V. Joseph, and N. V. Joshi, 1984: Ocean-atmosphere coupling over monsoon regions. *Nature*, **312**, 141–143, https://doi.org/10.1038/312141a0.

——, M. Rajeevan, and R. Nanjundiah, 2005: Monsoon prediction—Why yet another failure. *Curr. Sci.*, **88**, 1389–1400.

Goswami, B. N., 2005: South Asian monsoon. *Intraseasonal Variability in the Atmosphere-Ocean Climate System*, W. K. Lau and D. E. Waliser, Eds., Springer, 19–61.

——, S. A. Rao, D. Sengupta, and S. Chakravorty, 2016: Monsoons to mixing in the Bay of Bengal: Multiscale air-sea interactions and monsoon predictability. *Oceanography*, **29**, 18–27, https://doi.org/10.5670/oceanog.2016.35.

Graham, N., and T. Barnett, 1987: Sea surface temperature, surface wind divergence, and convection over tropical oceans. *Science*, **238**, 657–659, https://doi.org/10.1126/science.238.4827.657.

Hersbach, H., and Coauthors, 2020: The ERA5 global reanalysis. *Quart. J. Roy. Meteor. Soc.*, **146**, 1999–2049, https://doi.org/10.1002/qj.3803.

Holzworth, G. C., 1967: Mixing depths, wind speeds and air pollution potential for selected locations in the United States. *J. Appl. Meteor. Climatol.*, **6**, 1039–1044, https://doi.org/10.1175/1520-0450(1967)006<1039:MDWSAA>2.0.CO;2.

Hormann, V., L. R. Centurioni, and A. L. Gordon, 2019: Freshwater export pathways from the Bay of Bengal. *Deep-Sea Res. Part II*, **168**, 104645, https://doi.org/10.1016/j.dsr2.2019.104645.

Huffman, G. J., D. T. Bolvin, and E. J. Nelkin, 2015: Integrated Multi-satellitE Retrievals for GPM (IMERG) technical documentation. NASA/GSFC Code 612 Tech. Doc., 48 pp., http://pmm.nasa.gov/sites/default/files/document_files/IMERG_doc.pdf.

Hughes, K. G., J. N. Moum, and E. L. Shroyer, 2020: Heat transport through diurnal warm layers. *J. Phys. Oceanogr.*, **50**, 2885–2905, https://doi.org/10.1175/JPO-D-20-0079.1.

Iyengar, R. N., 2009: Monsoon rainfall cycles as depicted in ancient Sanskrit texts. *Curr. Sci.*, **97**, 444–447.

Jaeger, G. S., and A. Mahadevan, 2018: Submesoscale-selective compensation of fronts in a salinity-stratified ocean. *Sci. Adv.*, **4**, e1701504, https://doi.org/10.1126/sciadv.1701504.

Jensen, T. G., H. W. Wijesekera, E. S. Nyadjro, P. G. Thoppil, J. F. Shriver, K. K. Sandeep, and V. Pant, 2016: Modeling salinity exchanges between the equatorial Indian Ocean and the Bay of Bengal. *Oceanography*, **29**, 92–101, https://doi.org/10.5670/oceanog.2016.42.

Jiang, X., T. Li, and B. Wang, 2004: Structures and mechanisms of the northward propagating boreal summer intraseasonal oscillation. *J. Climate*, **17**, 1022–1039, https://doi.org/10.1175/1520-0442(2004)017<1022:SAMOTN>2.0.CO;2.

Kiladis, G. N., J. Dias, K. H. Straub, M. C. Wheeler, S. N. Tulich, K. Kikuchi, K. M. Weickmann, and M. J. Ventrice, 2014: A comparison of OLR and circulation-based indices for tracking the MJO. *Mon. Wea. Rev.*, **142**, 1697–1715, https://doi.org/10.1175/MWR-D-13-00301.1.

Klingaman, N. P., and S. J. Woolnough, 2014: Using a case-study approach to improve the Madden-Julian oscillation in the Hadley Centre model. *Quart. J. Roy. Meteor. Soc.*, **140**, 2491–2505, https://doi.org/10.1002/qj.2314.

——, and C. A. Demott, 2020: Mean state biases and interannual variability affect perceived sensitivities of the Madden-Julian oscillation to air-sea coupling. *J. Adv. Model. Earth Syst.*, **12**, e2019MS001799, https://doi.org/10.1029/2019MS001799.

——, S. J. Woolnough, H. Weller, and J. M. Slingo, 2011: The impact of finer-resolution air-sea coupling on the intraseasonal oscillation of the Indian monsoon. *J. Climate*, **24**, 2451–2468, https://doi.org/10.1175/2010JCLI3868.1.

Krishnamurti, T. N., and P. Ardanuy, 1980: The 10 to 20-day westward propagating mode and "Breaks in the Monsoons." *Tellus*, **32**, 15–26, https://doi.org/10.3402/tellusa.v32i1.10476.

Lee, C. M., and Coauthors, 2016: Collaborative observations of boundary currents, water mass variability, and monsoon response in the southern Bay of Bengal. *Oceanography*, **29**, 102–111, https://doi.org/10.5670/oceanog.2016.43.

Lee, S.-S., B. Wang, D. E. Waliser, J. M. Neena, and J.-Y. Lee, 2015: Predictability and prediction skill of the boreal summer intraseasonal oscillation in the intraseasonal variability hindcast experiment. *Climate Dyn.*, **45**, 2123–2135, https://doi.org/10.1007/s00382-014-2461-5.

Lucas, A. J., and Coauthors, 2016: Adrift upon a salinity-stratified sea: A view of upper-ocean processes in the Bay of Bengal during the southwest monsoon. *Oceanography*, **29**, 134–145, https://doi.org/10.5670/oceanog.2016.46.

MacKinnon, J. A., and Coauthors, 2016: A tale of two spicy seas. *Oceanography*, **29**, 50–61, https://doi.org/10.5670/oceanog.2016.38.

Mandke, S. K., P. A. Pillai, and A. K. Sahai, 2020: Simulation of monsoon intraseasonal oscillations in Geophysical Fluid Dynamics Laboratory models from Atmospheric Model Intercomparison Project integrations of Coupled Model Intercomparison Project phase 5. *Int. J. Climatol.*, **40**, 5574–5589, https://doi.org/10.1002/joc.6536.

McPhaden, M. J., and Coauthors, 2009: RAMA: The Research Moored Array for African-Asian-Australian Monsoon analysis and prediction. *Bull. Amer. Meteor. Soc.*, **90**, 459–480, https://doi.org/10.1175/2008BAMS2608.1.

Murty, G. R. K., 2014: India's romance with monsoon rains: A peep into poetic expressions and personal experiences. *IUP J. Engl. Stud.*, **9**, 54–73.

Neena, J. M., D. Waliser, and X. Jiang, 2017: Model performance metrics and process diagnostics for boreal summer intraseasonal variability. *Climate Dyn.*, **48**, 1661–1683, https://doi.org/10.1007/s00382-016-3166-8.

Pandit, R. S., 1944: *Kalidasa's Ritusamhara (The Pageant of the Seasons)*. The National Information & Publications Ltd, 95 pp.

Pinkel, R., and Coauthors, 2015: Breaking internal tides keep the ocean in balance. *Eos, Trans. Amer. Geophys. Union*, **96**, https://doi.org/10.1029/2015EO039555.

Prytherch, J., J. T. Farrar, and R. A. Weller, 2013: Moored surface buoy observations of the diurnal warm layer. *J. Geophys. Res. Oceans*, **118**, 4553–4569, https://doi.org/10.1002/jgrc.20360.

Puranik, S. S., K. C. S. Ray, P. N. Sen, and P. Pradeep Kumar, 2013: An index for predicting the onset of monsoon over Kerala. *Curr. Sci.*, **105**, 954–961.

Ramachandran, S., and Coauthors, 2018: Submesoscale processes at shallow salinity fronts in the Bay of Bengal: Observations during the winter monsoon. *J. Phys. Oceanogr.*, **48**, 479–509, https://doi.org/10.1175/JPO-D-16-0283.1.

Saha, S., and Coauthors, 2014: The NCEP Climate Forecast System version 2. *J. Climate*, **27**, 2185–2208, https://doi.org/10.1175/JCLI-D-12-00823.1.

——, A. Hazra, S. Pokhrel, H. S. Chaudhari, K. Sujith, A. Rai, H. Rahaman, and B. N. Goswami, 2019: Unraveling the mystery of Indian summer monsoon prediction: Improved estimate of predictability limit. *J. Geophys. Res. Atmos.*, **124**, 1962–1974, https://doi.org/10.1029/2018JD030082.

Sahai, A. K., R. Chattopadhyay, S. Joseph, P. M. Krishna, D. R. Pattanaik, and S. Abhilash, 2019: Seamless prediction of monsoon onset and active/break phases. *Sub-Seasonal to Seasonal Prediction*, A. W. Robertson, and F. Vitart, Eds., Elsevier, 421–438.

Schott, F. A., S.-P. Xie, and J. P. McCreary Jr., 2009: Indian Ocean circulation and climate variability. *Rev. Geophys.*, **47**, RG1002, https://doi.org/10.1029/2007RG000245.

Sengupta, D., B. R. Goddalehundi, and D. Anitha, 2008: Cyclone-induced mixing does not cool SST in the post-monsoon north Bay of Bengal. *Atmos. Sci. Lett.*, **9**, 1–6, https://doi.org/10.1002/asl.162.

Shroyer, E. L., D. L. Rudnick, J. T. Farrar, B. Lim, S. K. Venayagamoorthy, L. C. St. Laurent, A. Garanaik, and J. N. Moum, 2016: Modification of upper-ocean temperature structure by subsurface mixing in the presence of strong salinity stratification. *Oceanography*, **29**, 62–71, https://doi.org/10.5670/oceanog.2016.39.

Sikka, D. R., 2011: The role of the India Meteorological Department, 1875–1947. *History of Science, Philosophy and Culture in Indian Civilization, Volume XV, Part 4*, D. P. Chattopadhyaya, Ed., Pearson Education India, 381–429.

Sree Lekha, J., J. Buckley, A. Tandon, and D. Sengupta, 2018: Subseasonal dispersal of freshwater in the northern Bay of Bengal in the 2013 summer monsoon season. *J. Geophys. Res. Oceans*, **123**, 6330–6348, https://doi.org/10.1029/2018JC014181.

Stull, R. B., 1991: Static stability—An update. *Bull. Amer. Meteor. Soc.*, **72**, 1521–1530, https://doi.org/10.1175/1520-0477(1991)072<1521:SSU>2.0.CO;2.

Suhas, E., J. M. Neena, and B. N. Goswami, 2013: An Indian monsoon intraseasonal oscillations (MISO) index for real time monitoring and forecast verification. *Climate Dyn.*, **40**, 2605–2616, https://doi.org/10.1007/s00382-012-1462-5.

Thadathil, P., I. Suresh, S. Gautham, S. Prasanna Kumar, M. Lengaigne, R. Rao, S. Neetu, and A. Hegde, 2016: Surface layer temperature inversion in the Bay of Bengal: Main characteristics and related mechanisms. *J. Geophys. Res. Oceans*, **121**, 5682–5696, https://doi.org/10.1002/2016JC011674.

Thakur, R., E. L. Shroyer, R. Govindarajan, J. T. Farrar, R. A. Weller, and J. N. Moum, 2019: Seasonality and buoyancy suppression of turbulence in the Bay of Bengal. *Geophys. Res. Lett.*, **46**, 4346–4355, https://doi.org/10.1029/2018GL081577.

Todd, R. E., 2020: Equatorial circulation in the western Indian Ocean during onset of the 2018 summer monsoon and links to the Bay of Bengal. *Geophys. Res. Lett.*, **47**, e2020GL087215, https://doi.org/10.1029/2020GL087215.

Vecchi, G. A., and D. Harrison, 2002: Monsoon breaks and subseasonal sea surface temperature variability in the Bay of Bengal. *J. Climate*, **15**, 1485–1493, https://doi.org/10.1175/1520-0442(2002)015<1485:MBASSS>2.0.CO;2.

Venkatesan, R., V. R. Shamji, G. Latha, S. Mathew, R. R. Rao, A. Muthiah, and M. A. Atmanand, 2013: In situ ocean subsurface time-series measurements from OMNI buoy network in the Bay of Bengal. *Curr. Sci.*, **104**, 1166–1177.

Wijesekera, H. W., and Coauthors, 2015: Southern Bay of Bengal currents and salinity intrusions during the northeast monsoon. *J. Geophys. Res. Oceans*, **120**, 6897–6913, https://doi.org/10.1002/2015JC010744.

Woolnough, S. J., J. M. Slingo, and B. J. Hoskins, 2000: The relationship between convection and sea surface temperature on intraseasonal timescales. *J. Climate*, **13**, 2086–2104, https://doi.org/10.1175/1520-0442(2000)013<2086:TRBCAS>2.0.CO;2.

Xie, S.-P., H. Xu, N. Saji, Y. Wang, and W. T. Liu, 2006: Role of narrow mountains in large-scale organization of Asian monsoon convection. *J. Climate*, **19**, 3420–3429, https://doi.org/10.1175/JCLI3777.1.

Zhang, L., W. Han, Y. Li, and E. D. Maloney, 2018: Role of north Indian Ocean air–sea interaction in summer monsoon intraseasonal oscillation. *J. Climate*, **31**, 7885–7908, https://doi.org/10.1175/JCLI-D-17-0691.1.